Romanian Reports in Physics **72**, 414 (2020)

THEORETICAL UNDERSTANDING OF THE RESONANT INTERACTION BETWEEN TM_{01} AND HE_{12} MODES IN A LOSSY MODE FIBER-BASED PLASMONIC SENSOR

V. A. POPESCU[1,*], A. K. SHARMA[2]

[1] "Politehnica" University of Bucharest, Department of Physics 1, Splaiul Independentei 313, 060042 Bucharest, Romania
[*] Corresponding author, email: *vapopescu@yahoo.com*
[2] National Institute of Technology Delhi, Department of Applied Sciences, Physics Division, Narela, Delhi 110040, India

Received May 19, 2020

Abstract. A fiber-based plasmonic sensor with three layers is studied and the analytical method based on Bessel functions is applied to calculation of the loss, figure of merit, and amplitude and power sensitivities for the HE_{12} mode in a resonant interaction with a TM_{01} mode. In this method, the electromagnetic field is represented by a Bessel function J of the first kind in the core region (SiO_2), a linear combination of the Hankel functions H_1 and H_2 in the TiO_2/PSS (poly(styrene sulfonate)) region, and a modified Bessel function K of the second kind in the analyte region. The values of the effective indices calculated by using finite element method are in agreement with our analytical method. The results and subsequent analysis indicate that the full width at half maximum (FWHM) of the loss and maximum value of the loss P for HE_{12} mode in resonant interaction with a TM_{01} mode tend to decrease when the radius of the fiber core is increased. In addition, the shift $\delta\lambda_{res}$ towards longer wavelengths of the maximum loss P for an increase Δn_a of the analyte refractive index by 0.001 RIU, the figure of merit FOM, and the maximum of the amplitude S_A and power S_P sensitivities increase with fiber core radius. In the angular integration method, the power loss PL and the corresponding angle θ are increasing when the thickness d_2 of the lossy layer and the refractive index n_a of the analyte layer are increased. Also, the power loss PL increases and the corresponding angle θ decreases when the wavelength λ is increased.

Key words: sensor, optical fiber, plasmon, lossy mode, sensitivity.

1. INTRODUCTION

Optical fiber-based plasmonic sensors are widely used in chemical, biological, environmental monitoring, food safety, and medical diagnosis [1–31]. Thus, some plasmonic biosensors [1–7] have been applied for the detection of humidity, salivary cortisol, human-liver tissues, human blood groups (A, B, and O), and to measure the hemoglobin concentration in human blood.

In the technique of surface plasmon resonance (SPR), the wave vectors of the evanescent wave of the incident p-polarized beam and the surface plasmon wave (SPW) become identical and there takes place a transfer of energy from the incident beam to the SPW [8–14]. In recent time, SPR-based optical sensors have attained very high levels of performance. For example [11], in an SPR-based fiber optic sensor with six layers (ZBLAN fluoride core, 5 nm thick NaF clad, 60 nm thick amorphous Si layer, 45.3 nm thick Ag layer, 11 nm thick Al_2O_3 interlayer and heavy water as an analyte) and 938.7 nm wavelength, an extremely large figure of merit (FOM) of 31806.65 RIU^{-1} was obtained.

Another type of SPR takes place when the phase or loss matching conditions between a fundamental core mode and the corresponding plasmon mode are satisfied [15–23].

The lossy mode resonance (LMR) is due to the mode coupling between the guided modes in the fiber core and the lossy modes in the nanofilms when the real part of the thin-film permittivity is positive and higher in magnitude than both its own imaginary part and that of the material surrounding the thin-film [24–26]. As an example adapted from Ref. [25], in an LMR-based sensor (operated at 633 nm wavelength) with four layers: a BK7 prism with the refractive index (RI) $n_1 = 1.5151$, a 3 μm thick cytop with $n_2 = 1.34$, a 0.34 ×18 nm thick graphene with $n_3 = 3.0 + 1.1491i$, and an analyte with $n_4 = 1.335$, a large FOM of 581.8 RIU^{-1} is obtained for a TM mode. In Ref. [25], a maximum value of FOM as high as 410 RIU^{-1} has been reached, corresponding to a TM mode.

The values of the effective indices calculated by using the finite element method (FEM) are in agreement [27–31] with an analytical method where a linear combination of the Hankel functions H_1 and H_2 represents the field in the metallic region of a fiber-based plasmonic sensor. In addition, the difference between the resonant wavelengths calculated with the FEM and with the analytical method is negligibly small.

In this paper, an analytical method based on the Bessel functions, FEM, and an angular interrogation method are applied to an optical fiber-based plasmonic sensor when the dispersions of SiO_2 and TiO_2/PSS (poly(styrene sulfonate)) materials are considered. The values of the effective indices calculated by using FEM are in agreement with an analytical method, where the electromagnetic field is represented by a Bessel function J of the first kind in the core region (SiO_2), a linear combination of the Hankel functions H_1 and H_2 in the TiO_2/PSS region due to the complex value of the RI, and a modified Bessel function K of the second kind in the outermost (analyte) region.

The paper is structured as follows: In Section 2, we briefly present the structure of the three-layer optical fiber SPR sensor. The analytical method based on the Bessel functions and the angular interrogation method are described in Section 3 and Section 4, respectively. We discuss in Section 5 the results of numerical simulations. The summary of the obtained results is given in Section 6.

2. OPTICAL FIBER-BASED PLASMONIC SENSOR

Figure 1 shows an optical fiber with three layers (SiO_2, TiO_2/PSS, and analyte), where the thickness of the TiO_2/PSS layer is d_2.

The refractive index of SiO_2 is calculated through a Sellmeier-type relation [8]:

$$n = \sqrt{1 + \frac{0.6961663\lambda^2}{\lambda^2 - 0.0684043^2} + \frac{0.4079426\lambda^2}{\lambda^2 - 0.1162414^2} + \frac{0.8974794\lambda^2}{\lambda^2 - 9.896161^2}}\,. \tag{1}$$

The refractive index of the TiO_2/PSS [24] layer is calculated by the Drude model:

$$n = \sqrt{1 + \frac{61}{5.5^2 - \omega_1^2 - i \times 0.5 \times \omega_1}}\,, \tag{2}$$

where

$$\omega_1 = \frac{6.626075540 \times 10^{-34} \times 2.99792458 \times 10^{8}}{\lambda \times 10^{-6}} \times 6.241509 \times 10^{18} \tag{3}$$

and λ is in micrometers.

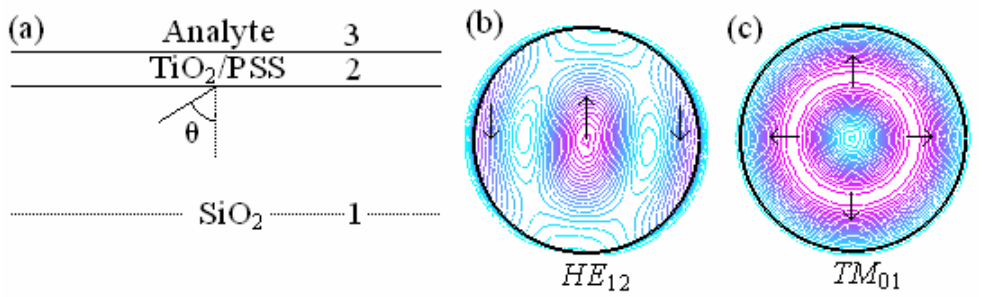

Fig. 1 – (a) Schematic of an optical fiber with three layers (SiO_2, TiO_2/PSS, and analyte). Further, the contour plot of the z-component $S_z(x, y)$ of the Poynting vector at the resonance (λ = 0.8494 μm) between the (b) HE_{12} and (c) TM_{01} modes when the fiber core radius is r_1 = 5 μm, the thickness of TiO_2/PSS lossy layer is d_2 = 70 nm, and the analyte RI is n_a = 1.333. The arrows in parts (b) and (c) show the electrical field orientation.

3. ADAPTED ANALYTICAL METHOD-BASED BESSEL FUNCTIONS

For a fiber structure with three layers [27–31], the complex propagation constant β at a modal index v is determined from the following dispersion equation:

$$\Delta = \begin{vmatrix} -\frac{u_1^{\,2}}{n_1^{\,2}} J(u_1 r_1) & 0 & -B_{12} & -B_{14} \\ -J'(u_1 r_1) & \frac{i\nu\beta}{\omega\mu_0 r_1} J(u_1 r_1) & -B_{22} & -B_{24} \\ 0 & u_1^{\,2} J(u_1 r_1) & -B_{32} & -B_{34} \\ -\frac{i\nu\beta}{\omega\varepsilon_0 n_1^{\,2} r_1} J(u_1 r_1) & -J'(u_1 r_1) & -B_{42} & -B_{44} \end{vmatrix} = 0 \tag{4}$$

where:

$$B_\nu = \begin{pmatrix} 0 & B_{12} & 0 & B_{14} \\ 0 & B_{22} & 0 & B_{24} \\ 0 & B_{32} & 0 & B_{34} \\ 0 & B_{42} & 0 & B_{44} \end{pmatrix} = M_1 M_2^{-1} M_f \tag{5}$$

$$M_1^{11} = -\frac{u_2^{\,2}}{n_2^{\,2}} H_1(u_2 r_1),\ M_1^{12} = -\frac{u_2^{\,2}}{n_2^{\,2}} H_2(u_2 r_1),\ M_1^{13} = 0,\ M_1^{14} = 0, \tag{6}$$

$$\begin{gathered} M_1^{21} = -H'_1(u_2 r_1),\ M_1^{22} = -H'_2(u_2 r_1), \\ M_1^{23} = \frac{i\nu\beta}{\omega\mu_0 r_1} H_1(u_2 r_1),\ M_1^{24} = \frac{i\nu\beta}{\omega\mu_0 r_1} H_2(u_2 r_1), \end{gathered} \tag{7}$$

$$M_1^{31} = 0,\ M_1^{32} = 0,\ M_1^{33} = u_2^{\,2} H_1(u_2 r_1),\ M_1^{34} = u_2^{\,2} H_2(u_2 r_1), \tag{8}$$

$$\begin{gathered} M_1^{41} = -\frac{i\nu\beta}{\omega\varepsilon_0 n_2^{\,2} r_1} H_1(u_2 r_1),\ M_1^{42} = -\frac{i\nu\beta}{\omega\varepsilon_0 n_2^{\,2} r_1} H_2(u_2 r_1), \\ M_1^{43} = -H'_1(u_2 r_1),\ M_1^{44} = -H'_2(u_2 r_1), \end{gathered} \tag{9}$$

$$M_2 = M_1(r_1 \to r_2), \tag{10}$$

$$M_f = \begin{pmatrix} 0 & \frac{w_3^{\,2}}{n_3^{\,2}} K(w_3 r_2) & 0 & 0 \\ 0 & -K'(w_3 r_2) & 0 & \frac{i\nu\beta}{\omega\mu_0 r_2} K(w_3 r_2) \\ 0 & 0 & 0 & -w_3^{\,2} K(w_3 r_2) \\ 0 & -\frac{i\nu\beta}{\omega\varepsilon_0 n_3^{\,2} r_2} K(w_3 r_2) & 0 & -K'(w_3 r_2) \end{pmatrix}, \tag{11}$$

$$u_1 = \sqrt{(kn_1)^2 - \beta^2}\ , u_2 = \sqrt{(kn_2)^2 - \beta^2}\ , w_3 = \sqrt{\beta^2 - (kn_3)^2}\ , \tag{12}$$

and where the prime represents the differentiation with respect to the radial variable r.

In order to evaluate the propagation characteristics, the z-component of the Poynting vector is defined by:

$$S_z = \frac{1}{2}\mathrm{Re}[E_x H_y^* - E_y H_x^*], \tag{13}$$

where E_x, H_x, E_y, and H_y represent the electric and magnetic components of the electromagnetic field along the x- and y-axes, respectively.

The loss in dB/cm is defined as:

$$P = \frac{40000\pi\beta_i}{k\lambda \ln(10)}\ , \tag{14}$$

where β_i is the imaginary part of the effective index.

The sensing performance of the device is determined by the local spectral sensitivity (S_λ) calculated for an increase of n_a with 0.001 RIU:

$$S_\lambda = \frac{\delta\lambda_{res}}{\delta n_a}, \quad \delta n_a = 0.001\ \mathrm{RIU}\ , \tag{15}$$

the signal-to-noise ratio (SNR):

$$\mathrm{SNR} = \frac{\delta\lambda_{res}}{\delta\lambda_{0.5}}, \tag{16}$$

the maximum of the local power sensitivity (S_P) calculated for an increase of n_a with 0.001 RIU:

$$S_P = \frac{\delta P}{\delta n_a}, \quad \delta n_a = 0.001\ \mathrm{RIU}\ , \tag{17}$$

the figure of merit (FOM):

$$\mathrm{FOM} = \frac{\delta\lambda_{res}}{\delta n_a \delta\lambda_{0.5}} \tag{18}$$

and the maximum of the amplitude sensitivity (S_A):

$$S_A = \frac{P_a - P}{\delta n_a} \times \frac{1}{P},\ \delta n_a = 0.001 \text{ RIU}, \tag{19}$$

where $\delta\lambda_{res}$ is the shift in resonance wavelength corresponding to a small variation δn_a in the RI of analyte, $\delta\lambda_{0.5}$ is the angular width of the resonance spectrum, P_a is the loss at $n_a + \delta n_a$, and P is the loss corresponding to reference analyte n_a.

For the variation of the real part of the RI (Δn_a^r = 0.001 RIU), the wavelength resonance shift is $\Delta\lambda_{res}$ and the resolution is defined as:

$$S_{R\lambda} = \frac{\Delta n_a^r}{\Delta\lambda_{res}} \Delta\lambda_L. \tag{20}$$

Here, it is assumed that the wavelength detection limit is $\Delta\lambda_L$ = 0.001 nm. For Δn_a^r = 0.001 RIU, the loss shift is ΔP_{res} and the power resolution (limit of detection) is given as:

$$S_{RP} = \frac{\Delta n_a^r}{\Delta P_{res}} \Delta P_L. \tag{21}$$

For Eq. (21), it is assumed that the power detection limit (resolution of power measurement) is ΔP_L = 0.01 dB/cm.

4. ADAPTED ANGULAR INTERROGATION METHOD

In the angular interrogation method [8–14], a resonant interaction between an incident wave vector and the surface plasmon wave-vector (TM plasmonic mode) is analyzed. In this method, the wavelength is kept constant and the angle of incidence is varied until a maximum of the power loss appears at a resonance incidence angle θ. The resonance incidence angle depends on the RI of the sensing (*i.e.*, analyte) medium.

The power loss (in dB) corresponding to a TM mode in fiber with N = 3 layers is [11]:

$$PL = 10\ \log\frac{1}{P_o}, \tag{22}$$

where P_o is the output power and is calculated as:

$$P_o = R^{\frac{L}{D\tan(\theta)}}. \tag{23}$$

In Eq. (23), L is the sensing length, D is the fiber core diameter, θ is the angle inside the fiber (L/D = 25), and R is the corresponding intensity reflection coefficient calculated as:

$$R = |r|^2, \tag{24}$$

where r is the amplitude reflection coefficient calculable from the transfer matrix method (TMM) [32]:

$$r = \frac{(M_{11} + M_{12}q_3)q_1 - (M_{21} + M_{22}q_3)}{(M_{11} + M_{12}q_3)q_1 + (M_{21} + M_{22}q_3)}. \tag{25}$$

In the above relation we have

$$M_2 = \begin{pmatrix} M_{11} & M_{12} \\ M_{21} & M_{22} \end{pmatrix}, \tag{26}$$

where

$$M_2 = \begin{pmatrix} \cos\beta_2 & -\dfrac{i\sin\beta_2}{q_2} \\ -iq_2\sin\beta_2 & \cos\beta_2 \end{pmatrix}, \tag{27}$$

$$q_1 = \sqrt{n_1^2 - n_1^2\sin^2\theta}, q_2 = \sqrt{n_2^2 - n_1^2\sin^2\theta}, q_3 = \sqrt{n_3^2 - n_1^2\sin^2\theta} \tag{28}$$

$$\beta_2 = \frac{2\pi d_2}{\lambda}\sqrt{n_2^2 - n_1^2\sin^2\theta}. \tag{29}$$

The real part of the propagation constant of the SPW is given by the relation:

$$\mathrm{Re}\,\beta = \frac{2\pi}{\lambda}n_1\sin\theta = \frac{2\pi}{\lambda}\sqrt{\frac{\varepsilon_r n_a^{\,2}}{\varepsilon_r + n_a^{\,2}}}, \tag{30}$$

where n_1 is the RI of the core layer (SiO_2), θ is the angle inside the fiber, ε_r is the real part of the TiO_2/PSS dielectric function, and n_a is the real part of the analyte RI.

For a wavelength λ = 0.8494 μm, n_1 = 1.452508, θ = 47.373392°, ε_r = 3.167863 > $n_1^2 > n_a^2 > \varepsilon_i$, and n_a = 1.333,

$$\frac{2\pi}{\lambda} n_1 \sin\theta = 7.905614, \quad \frac{2\pi}{\lambda}\sqrt{\frac{\varepsilon_r n_a^2}{\varepsilon_r + n_a^2}} = 7.892393. \tag{31}$$

For the same values of λ, n_1, ε_r , and n_a , Eq. (30) gives θ = 47.269392°, a value close to that calculated with the TMM from the angular interrogation method, *i.e.*, θ = 47.373392° for a *TM* mode. We remember that Eq. (30) is valid for the case where two media (SiO_2 and TiO_2/PSS) are semi-infinite.

The sensing performance of the device is determined by the local angular sensitivity (S_θ) calculated for an increase of n_a with 0.001 RIU:

$$S_\theta = \frac{\delta\theta_{res}}{\delta n_a}, \quad \delta n_a = 0.001 \text{ RIU}, \tag{32}$$

the signal-to-noise ratio (SNR):

$$\text{SNR} = \frac{\delta\theta_{res}}{\delta\theta_{0.5}}, \tag{33}$$

the maximum of the local power sensitivity (S_{PL}) calculated for an increase of n_a with 0.001 RIU:

$$S_{PL} = \frac{\delta PL}{\delta n_a}, \quad \delta n_a = 0.001 \text{ RIU}, \tag{34}$$

the figure of merit (FOM):

$$\text{FOM} = \frac{\delta\theta_{res}}{\Delta n_a \delta\theta_{0.5}}, \tag{35}$$

and the maximum of the amplitude sensitivity (S_A):

$$S_A = \frac{PL_a - PL}{\delta n_a} \times \frac{1}{PL}, \quad \delta n_a = 0.001 \text{ RIU}, \tag{36}$$

where $\delta\theta_{res}$ is the shift in resonance angle corresponding to small variation δn_a in the analyte RI, $\delta\theta_{0.5}$ is the angular width of resonance spectrum, PL_a is the power loss at $n_a + \delta n_a$, and PL is power loss corresponding to reference analyte n_a.

For the variation of real part of the refractive index (Δn_a^r = 0.001 RIU), the angular resonance shift is $\Delta\theta_{res}$ and the resolution is:

$$S_{R\theta} = \frac{\Delta n_a^r}{\Delta\theta_{res}} \Delta\theta_L. \tag{37}$$

In Eq. (37), it is assumed that the angular (wavelength) detection limit is $\Delta\theta_L = 0.001^o$. For Δn_a^r = 0.001 RIU, the power loss shift is $\Delta P_{L\text{res}}$ and the power loss resolution (limit of detection in intensity interrogation mode) is:

$$S_{RPL} = \frac{\Delta n_a^r}{\Delta PL_{res}} \Delta PL_L. \tag{38}$$

In Eq. (38), it is assumed that the power detection limit (resolution of power measurement) is $\Delta PL_L = 0.01$ dB.

5. NUMERICAL RESULTS AND DISCUSSION

Figure 2 shows the imaginary part of the effective index, the loss, and the real part of the effective index *versus* the wavelength λ for the modes HE_{12} and TM_{01} when the radius of the fiber core is r_1 = 2.5 μm, the thickness of the lossy layer is d_2 = 70 nm and the RI of the analyte is n_a = 1.333. The maximum of the imaginary part of the effective index is at λ = 0.8262 μm, where $\delta\lambda_{res}$ = 1.8 nm, S_λ = 1800 nm/RIU, $\delta\lambda_{0.5}$ = 511 nm, FOM = 3.52 RIU^{-1} and P = 686.2 dB/cm. The maximum of the loss is at a shorter wavelength (λ = 0.8098 μm), where $\delta\lambda_{res}$ = 1.6 nm, S_λ = 1600 nm/RIU, $\delta\lambda_{0.5}$ = 371 nm, FOM = 4.31 RIU^{-1}, P = 693.4 dB/cm, S_A = 13.34 RIU^{-1}, λ_A = 0.74 μm, $\delta\lambda_A$ = 68.6 nm, S_P = 7454.6 dB/cmRIU, λ_P = 0.7563 μm, $\delta\lambda_P$ = 53.5 nm, and $S_{RP} = 1.34\times10^{-6}$ RIU. The phase matching condition is at a shorter wavelength (λ = 0.7875 μm). Figure 3 shows the same characteristics as in Fig. 2 but for n_a = 1.334. The maximum of the imaginary part of the effective index is at λ = 0.8280 μm where FWHM = 514 nm and the maximum of the loss is at a smaller wavelength (λ = 0.8114 μm), where FWHM = 373 nm. The phase matching condition is at λ = 0.7885 μm.

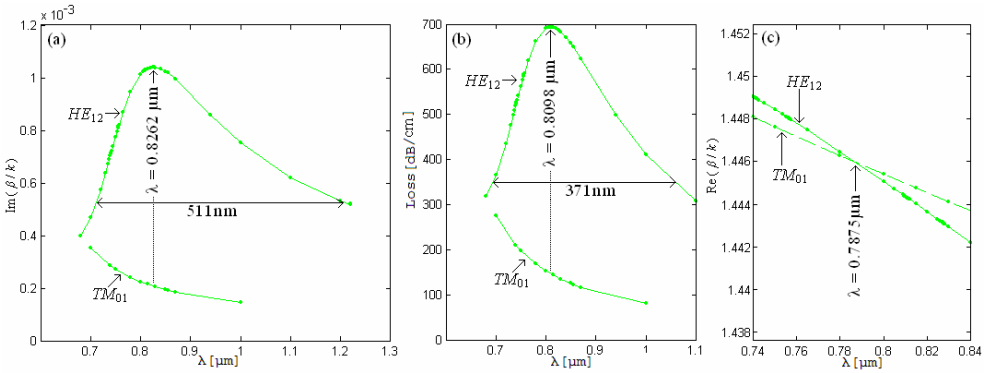

Fig. 2 – Imaginary part of (a) effective index, (b) loss, and (c) real part of the effective index *versus* wavelength (λ) for the modes HE_{12} and TM_{01} when the radius of the fiber core is r_1 = 2.5 μm, the thickness of the lossy layer is d_2 = 70 nm, and the analyte RI is n_a = 1.333.

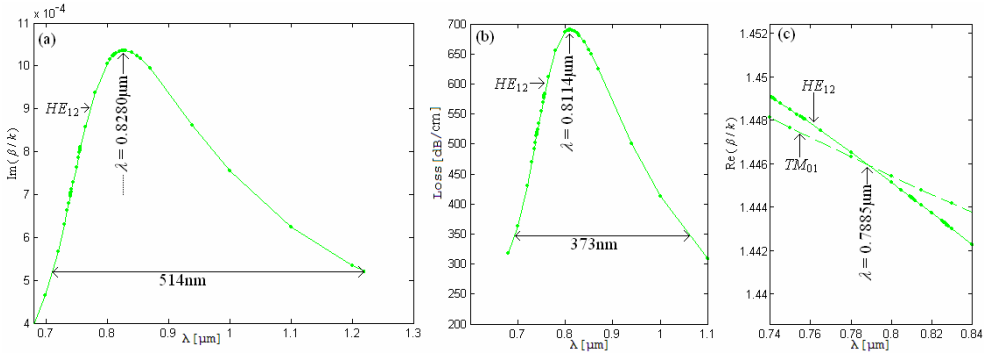

Fig. 3 – Imaginary part of (a) effective index, (b) loss, and (c) real part of the effective index *versus* wavelength (λ) for the modes HE_{12} and TM_{01} when the radius of the fiber core is r_1 = 2.5 μm, the thickness of the lossy layer is d_2 = 70 nm, and the analyte RI is n_a = 1.334.

Figure 4 shows the imaginary part of the effective index, the loss, and the real part of the effective index *versus* the wavelength λ for the modes HE_{12} when the radius of the fiber core is r_1 = 5 μm, the thickness of the lossy layer is d_2 = 70 nm, and the analyte RI is n_a = 1.333. The maximum of the imaginary part of the effective index is at λ = 0.8546 μm where $\delta\lambda_{res}$ = 2.3 nm, S_λ = 2300 nm/RIU, $\delta\lambda_{0.5}$ = 245 nm, FOM = 9.40 RIU^{-1}, and P = 338.7 dB/cm. The maximum of the loss is at a shorter wavelength (λ = 0.8494 μm), where $\delta\lambda_{res}$ = 2.1 nm, S_λ = 2100 nm/RIU, $\delta\lambda_{0.5}$ = 208 nm, FOM = 10.09 RIU^{-1}, P = 339.8 dB/cm, S_A = 34.69 RIU^{-1}, λ_A = 0.80 μm, $\delta\lambda_A$ = 52 nm, S_P = 8348.6 dB/cmRIU, λ_P = 0.8123 μm, $\delta\lambda_P$ = 37.1 nm, and $S_{RP} = 1.20\times10^{-6}$ RIU. The phase matching condition is at a shorter wavelength (λ = 0.8553 μm). Figure 5 shows the same characteristics as in Fig. 4 but for n_a = 1.334. The maximum of the imaginary part of the effective index is at λ = 0.8569 μm, where FWHM = 246 nm.

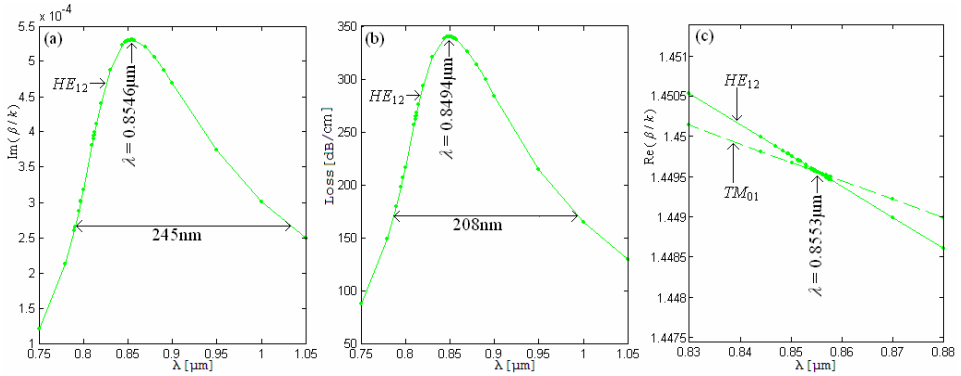

Fig. 4 – Imaginary part of (a) effective index, (b) loss, and (c) real part of the effective index *versus* wavelength (λ) for the mode HE_{12} when the radius of the fiber core is $r_1 = 5$ μm, the thickness of the lossy layer is $d_2 = 70$ nm, and the analyte RI is $n_a = 1.333$.

The maximum of the loss is at a shorter wavelength (λ = 0.8515 μm), where FWHM = 209 nm. The phase matching condition is at λ = 0.8573 μm.

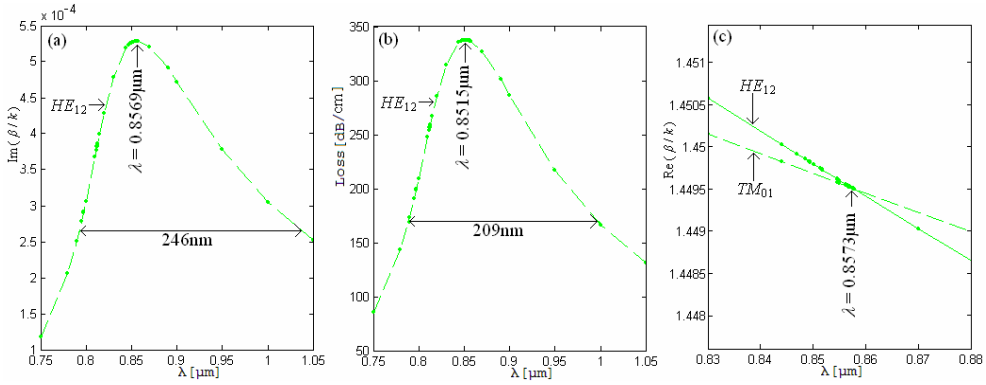

Fig. 5 – Imaginary part of (a) effective index, (b) loss, and (c) real part of the effective index *versus* wavelength (λ) for the mode HE_{12} when the radius of the fiber core is $r_1 = 5$ μm, the thickness of the lossy layer is $d_2 = 70$ nm, and the analyte RI is $n_a = 1.334$.

Figure 6 shows the similar characteristics (as shown in Fig. 5) for the modes HE_{12} and TM_{01} when the radius of the fiber core is $r_1 = 5$ μm, the thickness of the lossy layer is $d_2 = 70$ nm, and the analyte RI is $n_a = 1.363$. The maximum of the imaginary part of the effective index is at λ = 0.9393 μm, where $\delta\lambda_{res} = 3.6$ nm, $S_\lambda = 3600$ nm/RIU, $\delta\lambda_{0.5} = 370$ nm, FOM = 9.73 RIU^{-1} and $P = 272.6$ dB/cm. The loss is at a shorter wavelength (λ = 0.9295 μm), where $\delta\lambda_{res} = 3.3$ nm, $S_\lambda = 3300$ nm/RIU, $\delta\lambda_{0.5} = 296$ nm, FOM = 11.15 RIU^{-1}, $P = 274.1$ dB/cm, $S_A = 36.30$ RIU^{-1}, $\lambda_A = 0.8580$ μm, $\delta\lambda_A = 72$ nm, $S_P = 7240.9$ dB/cm RIU, $\lambda_P = 0.8780$ μm, $\delta\lambda_P = 51.5$ nm, and $S_{RP} = 1.4 \times 10^{-6}$ RIU. The phase matching condition is at a shorter wavelength (λ = 0.9269 μm). For $n_a = 1.364$, the maximum of the imaginary part of the

effective index is at λ = 0.9429 μm, where FWHM = 377 nm and the maximum of the loss is at a smaller wavelength (λ = 0.9328 μm), where FWHM = 301 nm.

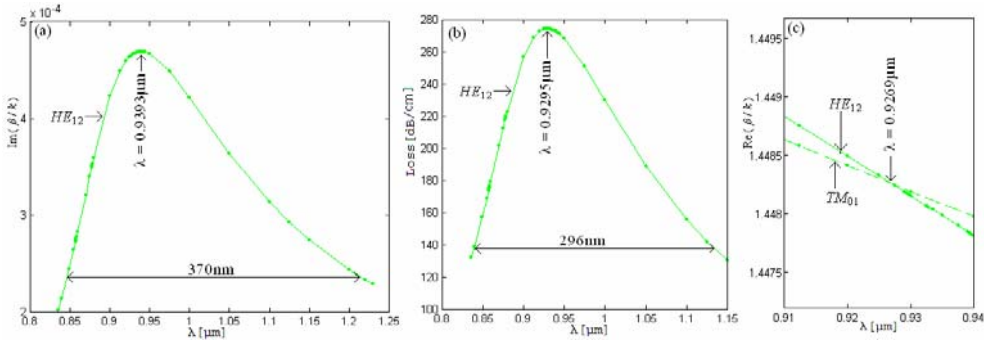

Fig. 6 – Imaginary part of (a) effective index, (b) loss, and (c) real part of the effective index *versus* wavelength (λ) for the mode HE_{12} when the radius of the fiber core is r_1 = 5 μm, the thickness of the lossy layer is d_2 = 70 nm, and the analyte RI is n_a = 1.363.

Figure 7 shows the loss *versus* the wavelength λ for the mode HE_{12} for different radii of the fiber core, *i.e.*, r_1 = 2.5 μm (FWHM = 371 nm, P = 693.4 dB/cm, $\delta\lambda_{res}$ = 1.6 nm), r_1 = 5 μm (FWHM = 208 nm, P = 339.8 dB/cm, $\delta\lambda_{res}$ = 2.1 nm), r_1 = 7.5 μm (FWHM = 135 nm, P = 234.4 dB/cm, $\delta\lambda_{res}$ = 2.3 nm), and r_1 = 10 μm (FWHM = 91 nm, P = 189.5 dB/cm, $\delta\lambda_{res}$ = 2.5 nm), the lossy layer thickness is d_2 = 70 nm and the analyte RI is n_a = 1.333. The full width at half maximum (FWHM) of the loss and the maximum value of the loss P for the HE_{12} mode in resonant interaction with the TM_{01} mode decrease when the fiber core radius is increased. For this mode, there is observed a larger shift towards longer wavelengths of the maximum loss P for an increase Δn_a of the analyte RI by 0.001 RIU.

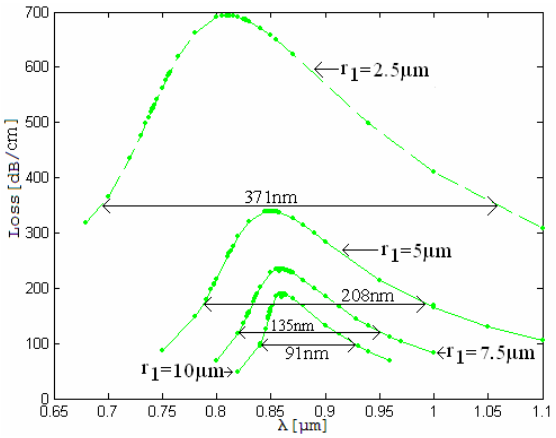

Fig. 7 – Loss *versus* wavelength λ for the mode HE_{12} for different values of fiber core radius, *i.e.*, r_1 = 2.5 μm, r_1 = 5 μm, r_1 = 7.5 μm, and r_1 = 10 μm. The thickness of the lossy layer is d_2 = 70 nm and the analyte RI is n_a = 1.333.

Figure 8 shows the amplitude and power sensitivities *versus* the wavelength λ for the mode HE_{12} for different values of fiber core radius, *i.e.*, $r_1 = 2.5$ μm, $r_1 = 5$ μm, 7.5 μm, and 10 μm. The thickness of the lossy layer is $d_2 = 70$ nm and the analyte RI is $n_a = 1.333$. It is clearly visible that the maxima of the amplitude (S_A) and the power (S_P) sensitivities increase for greater values of fiber core radius (r_1).

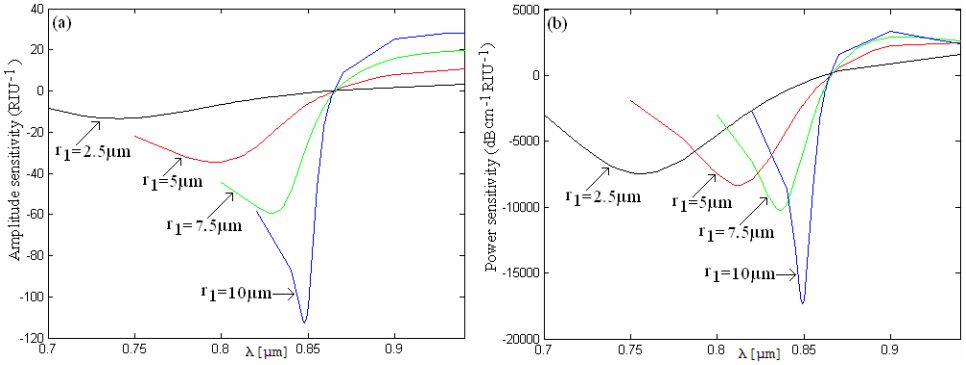

Fig. 8 – Amplitude sensitivity (a) and power sensitivity (b) *versus* the wavelength λ for the mode HE_{12} for different values of fiber core radius, *i.e.*, $r_1 = 2.5$ μm, $r_1 = 5$ μm, 7.5 μm, and 10 μm, the thickness of the lossy layer is $d_2 = 70$ nm and the analyte RI is $n_a = 1.333$.

Figure 9 shows the variation of resonance wavelength (corresponding to the imaginary part of the effective index and loss) *versus* thickness d_2 of the lossy layer for the mode HE_{12} when the radius of the fiber core is $r_1 = 5$ μm, and the analyte RI is $n_a = 1.333$. One can observe that the resonance wavelength is extremely sensitive as it increases linearly with an increase in the lossy layer thickness. It can also be observed that the resonance wavelength corresponding to the imaginary part of the effective index, and the loss for the HE_{12} mode undergo a 10 nm and 14 nm redshift, respectively.

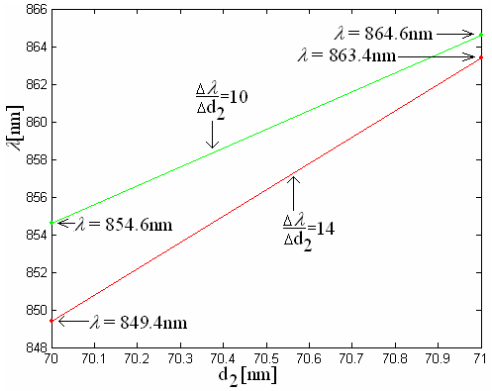

Fig. 9 – Resonance wavelength λ of the imaginary part of the effective index (green curve) and loss (red curve) *versus* the thickness d_2 of the lossy layer for the mode HE_{12} when the radius of the fiber core is $r_1 = 5$ μm, and the analyte RI is $n_a = 1.333$ (Color online).

Figures 10 a, b, and c show the λ-dependent, d_2-dependent, and n_a-dependent simulated variations of the power loss PL (left vertical axis) and the corresponding angle θ (right vertical axis) in the angular interrogation method. These results indicate that the power loss PL and the corresponding angle θ are increasing with any increase in thickness (d_2) of the lossy layer and the RI (n_a) of the analyte layer. However, with an increase in wavelength (λ), the power loss (PL) increases whereas the corresponding angle θ decreases.

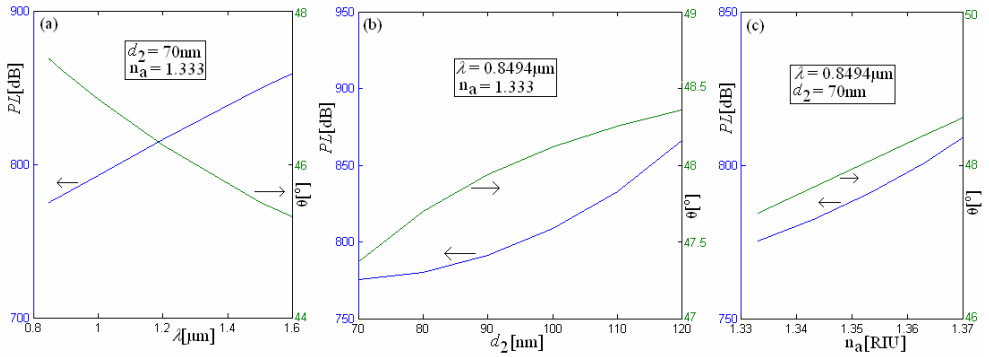

Fig. 10 – Power loss P_L (left) and corresponding angle θ (right) *versus* (a) wavelength (λ), (b) thickness of the lossy layer (d_2), and (c) analyte RI (n_a) in the angular interrogation method.

Table 1 shows the shift $\delta\theta_{res}$ towards higher angles of the maximum power loss P_L for an increase Δn_a of the analyte refractive index by 0.001 RIU, the full width at half maximum (FWHM) of the angular loss $\delta\theta_{0.5}$, the figure of merit (FOM), the maximum of the amplitude sensitivity S_A, the maximum value of the power loss PL, the angle θ inside the fiber, and the wavelength λ for a TM mode of a fiber where d_2 is the thickness of the lossy layer and n_a is the refractive index of the analyte in the angular interrogation method. The line shape of the angle-dependent power loss is asymmetric for a TM mode.

Table 1

Values of $\delta\theta_{res}$ [°], $\delta\theta_{0.5}$ [°], FOM [RIU^{-1}], S_A [RIU^{-1}], S_P [dB/RIU], PL [dB], θ [°], and λ [μm] for a TM mode of an optical fiber with three layers where the thickness of the lossy layer is d_2 [nm] and the RI of the analyte layer is n_a. The line shape of the angle-dependent power loss is assumed symmetric

d_2	n_a	$\delta\theta_{res}$	$\delta\theta_{0.5}$	FOM	S_A	S_P	P_L	θ	λ
70	1.333	0.034	13.31	2.59	4.26	696.5	775.2	47.37	0.8494
70	1.333	0.035	13.38	2.59	4.26	653.6	776.2	47.34	0.8583
90	1.333	0.029	11.28	2.58	4.45	733.1	791.1	47.94	0.8494
70	1.363	0.033	12.64	2.62	4.43	1105.9	800.8	48.39	0.8494

Table 2 shows the shift $\delta\lambda_{res}$ towards longer wavelengths of the maximum loss P for an increase Δn_a of the analyte refractive index by 0.001 RIU, the full

width at half maximum $\delta\lambda_{0.5}$ of the loss, the figure of merit FOM, the maximum of the amplitude S_A and the power S_P sensitivities, the maximum value of the loss P, the resonant wavelength λ, the wavelength λ_A for S_A, and the wavelength λ_P for S_P for a HE_{12} mode, where r_1 is the radius of fiber core, $d_2 = 70$ nm is the thickness of the lossy layer and $n_a = 1.333$ is the refractive index of the analyte in the analytical method based on the Bessel functions.

Table 2

Values of $\delta\lambda_{res}$ [nm], $\delta\lambda_{0.5}$ [nm], FOM [RIU^{-1}], S_A [RIU^{-1}], S_P [dB/cmRIU], P [dB/cm], λ [μm], λ_A [μm], and λ_P [μm] for a HE_{12} mode of an optical fiber with three layers where the radius of fiber core is r_1 [μm], the thickness of the lossy layer is $d_2 = 70$ nm, and the RI of the analyte layer is $n_a = 1.333$

r_1	$\delta\lambda_{res}$	$\delta\lambda_{0.5}$	FOM	S_A	S_P	P	λ	λ_A	λ_P
2.5	1.6	371	4.31	13.3	7454.6	693.4	0.8098	0.7412	0.7563
5.0	2.1	208	10.09	34.7	8348.6	339.8	0.8494	0.7974	0.8123
7.5	2.3	135	17.04	50.5	10241.0	234.4	0.8583	0.8293	0.8362
10	2.5	91	27.47	112.6	17334.0	189.5	0.8600	0.8480	0.8493

6. CONCLUSIONS

The analytical method based on the Bessel functions show that for an optical fiber-based LMR sensor with only three layers, the best values of S_λ, $\delta\lambda_{0.5}$, FOM, S_A, S_P, $S_{R\lambda}$, and S_{RP} for the HE_{12} mode in resonant interaction with the TM_{01} mode, are obtained when the radius of the fiber core is increased from $r_1 = 2.5$ μm to $r_1 = 10$ μm. Thus, when r_1 is increased (2.5 μm, 5 μm, 7.5 μm, and 10 μm), the local spectral sensitivity S_λ increases (1600 nm/RIU, 2100 nm/RIU, 2300 nm/RIU, and 2500 nm/RIU), the full width $\delta\lambda_{0.5}$ at half maximum of the loss decreases (371 nm, 208 nm, 135 nm, and 91 nm), the figure of merit FOM increases (4.31 RIU^{-1}, 10.09 RIU^{-1}, 17.04 RIU^{-1}, and 27.47 RIU^{-1}), the maximum of the amplitude sensitivity S_A increases (13.3 RIU^{-1}, 34.7 RIU^{-1}, 50.5 RIU^{-1}, and 112.6 RIU^{-1}), the maximum of the local power sensitivity S_P increases (7454.6 dB $cm^{-1}RIU^{-1}$, 8348.6 dB $cm^{-1}RIU^{-1}$, 10241.0 dB $cm^{-1}RIU^{-1}$, and 17334.0 dB $cm^{-1}RIU^{-1}$), the power resolution (limit of detection) S_{RP} gets finer (1.34×10^{-6} RIU, 1.20×10^{-6} RIU, 9.76×10^{-7} RIU, and 5.77×10^{-7} RIU) and the resonance wavelength undergoes a red-shift (0.8098 μm, 0.8494 μm, 0.8583 μm, and 0.8600 μm), respectively. Also, the spectral resolution $S_{R\lambda}$ is 4.35×10^{-7} RIU for $r_1 = 7.5$ μm and 4.0×10^{-7} RIU for $r_1 = 10$ μm.

For the same value of the analyte RI, the power resolution (5.77×10^{-7} RIU) for $r_1 = 10$ μm is significantly finer than the power loss resolution (1.52×10^{-5} RIU) in the angular interrogation mode.

We have studied for the first time, to the best of our knowledge, a resonant interaction between a HE_{12} mode and a TM_{01} mode. We believe that our results can be further improved by increasing the number of layers whose materials, thicknesses,

and optical properties are specifically designed to maximize the sensitivity and other performance parameters of the sensor.

REFERENCES

1. A. K. Sharma, B. Kaur, and V. A. Popescu, Opt. Mater. **102**, 109824 (2020).
2. A. K. Pandey, A. K. Sharma, and C. Marques, Materials **13**, 1623 (2020).
3. V. A. Popescu and A. K. Sharma, Opt. Quant. Electron. **51**, 290 (2019).
4. V. A. Popescu and A. K. Sharma, Sens. Imaging **21**, 5 (2020).
5. V. A. Popescu, Plasmonics **12**, 1733 (2017).
6. V. A. Popescu, Plasmonics **13**, 575 (2018).
7. V. A. Popescu, Plasmonics **13**, 1507 (2018).
8. A. K. Sharma, R. Jha, and B. D. Gupta, Opt. Commun. **274**, 320 (2007).
9. A. K. Sharma and G. J. Mohr, New J. Phys. **10**, 023039 (2008).
10. B. D. Gupta and R. K. Verma, J. Sens. **979761**, 1 (2009).
11. A. K. Sharma, A. Dominic, B. Kaur, and V. A. Popescu, J. Lightwave Technol. **37**, 5641 (2019).
12. V. A. Popescu, Rom. J. Phys. **64**, 202 (2019).
13. V. A. Popescu, Rom. Rep. Phys. **71**, 408 (2019).
14. V. A. Popescu, Rom. Rep. Phys. **72**, 407 (2020).
15. V. A. Popescu, N. N. Puscas, and G. Perrone, J. Opt. Soc. Am. B **29**, 3039 (2012).
16. V. A. Popescu, N. N. Puscas, and G. Perrone, J. Opt. Soc. Am. B **31**, 1062 (2014).
17. V. A. Popescu, N. N. Puscas, and G. Perrone, J. Opt. Soc. Am. B **32**, 473 (2015).
18. V. A. Popescu, N. N. Puscas, and G. Perrone, Plasmonics **11**, 1183 (2016).
19. V. A. Popescu, N. N. Puscas, and G. Perrone, Plasmonics **12**, 905 (2017).
20. V. A. Popescu, Rom. J. Phys. **62**, 204 (2017).
21. V. A. Popescu, N. N. Puscas, and G. Perrone, J. Opt. **19**, 075004 (2017).
22. V. A. Popescu, N. N. Puscas, and G. Perrone, Optics **6**, 21 (2017).
23. V. A. Popescu, J. Phys. Commun. **2**, 015029 (2018).
24. W.-M. Zhao, Q. Wang, X.-Z. Wang, X. Li, J.-Y.Jing, and H.-Z. A. Sun, J. Opt. Soc. Am. B **36**, 2069 (2019).
25. Y. Zhao, L. Wu, S. Gan, B. Ruan, J. Zhu, X. Dai, and Y. Xiang, Plasmonics **14**, 929 (2019).
26. N. Paliwal and J. John, IEEE Sensors J. **15**, 5361 (2015).
27. V. A. Popescu, J. Supercond. Nov. Magn. **25**, 1 (2012).
28. V. A. Popescu, J. Supercond. Nov. Magn. **25**, 143 (2012).
29. V. A. Popescu, J. Supercond. Nov. Magn. **25**, 1413 (2012).
30. V. A. Popescu, N. N. Puscas, and G. Perrone, Mod. Phys. Lett. B **30**, 1650075 (2016).
31. V. A. Popescu, Rom. Rep. Phys. **70**, 404 (2018).
32. E. Hecht, *Optics,* 4ed., Pearson Education, 2002.